JOURNAL OF CATALYSIS 93, 442–450 (1985)

Precursors of the Copper–Zinc Oxide Methanol Synthesis Catalysts

P. B. HIMELFARB, G. W. SIMMONS, K. KLIER, AND R. G. HERMAN

Departments of Chemistry and Materials Science and Metallurgical Engineering, and Center for Surface and Coatings Research, Lehigh University, Bethlehem, Pennsylvania 18015

Received October 3, 1984

The coprecipitated hydroxycarbonate precursor of the methanol synthesis and shift reaction catalyst based on 30 at.% copper and 70 at.% zinc oxide, which was previously reported to be a mixture of hydrozincite $Zn_5(CO_3)_2(OH)_6$ and rosasite $(Cu,Zn)_2(CO_3)(OH)_2$ (R. G. Herman, K. Klier, G. W. Simmons, B. P. Finn, J. B. Bulko, and T. P. Kobylinski, *J. Catal.* **56,** 407, 1979) or a single-phase hydrozincite (G. Petrini, F. Montino, A. Bossi, and G. Gaybassi, *in* "Studies in Surface Science and Catalysis. Preparation of Catalysis III" (G. Poncelet, P. Grange, and P. A. Jacobs, Eds.), Vol. 16, p . 735. Elsevier, The Netherlands, 1983), is herein shown to be a single-phase aurichalcite $(Cu_{0.3}Zn_{0.7})_5(CO_3)_2(OH)_6$. The orthorhombic $B22_12$ aurichalcite is crystallograpically distinct from the monoclinic $C2/m$ hydrozincite, although these two compounds have the same ratio of metal ions to carbonate and hydroxyl anions. Both aurichalcite and hydrozincite are chemically and structurally distinct from the monoclinic $P2_1/a$ rosasite. The earlier erroneous assignments are attributed to the structural similarity of the three hydroxycarbonates in question. An energy-dispersive characteristic X-ray emission analysis of individual particles in the scanning transmission electron microscope reveals a uniform distribution of copper and zinc at the analytical concentration Cu/Zn = 30/70. Precursors with less than 30% copper consist of mixtures of aurichalcite and hydrozincite.

INTRODUCTION

The structure and composition of coprecipitated precursors of the binary copper–zinc oxide methanol synthesis and shift catalysts have been reexamined, and the results presented herein correct some previous erroneous assignments. In an earlier communication from this laboratory, Herman *et al.* (*1*) reported the precursors coprecipitated from copper and zinc nitrate solutions by sodium carbonate to be a mixture of hydrozincite (*H*) $Zn_5(CO_3)_2(OH)_6$ and rosasite (*R*) $(Cu,Zn)_2CO_3(OH)_2$ for the atomic ratio Cu/Zn = 30/70, and mixtures of *H*, *R*, and copper hydroxide nitrate (*CuHN*) $Cu_2(OH)_3NO_3$ at all other Cu/Zn ratios. On the other hand, Petrini *et al.* (*2*) reported the precursor to be a single-phase *H* when the Cu/Zn ratio was less than or equal to 31/69, and a mixture of *H* and *CuHN* for Cu/Zn ratios greater than 31/69. All of these previous assignments were based on X-ray powder diffraction (XRD). Aside from difficulties with the XRD analysis of multiphase powdered specimens, this technique alone sometimes gives ambiguous results for structurally and chemically related compounds. In the group of hydroxycarbonates of copper and zinc, for example, the monoclinic *H* and orthorhombic aurichalcite (*A*) have very similar XRD patterns (*3*), and the difficulty in distinguishing the *H* and *A* phases was recently noted by Busetto *et al.* (*4*) in a study of coprecipitated Cu/Zn/Al hydroxycarbonates. These authors observed "quasi-amorphous" phases which were attributed to either *H* or *A* in samples with low Al loading. An unambiguous identification of synthetically prepared *A* has not been reported in the literature.

In the present work, the XRD analyses were supplemented by an electron diffraction study, using selected area (SAD) and convergent beam (CBD) diffraction in the

0021-9517/85 $3.00

transmission electron microscope (TEM) and the energy-dispersive X-ray spectroscopic (EDS) analysis in the scanning transmission electron microscope (STEM). The results of the X-ray and electron diffraction observations show that the catalyst precursor contains a single-phase aurichalcite *A* of the composition $Cu_{1.5}Zn_{3.5}(CO_3)_2(OH)_6$ for the Cu/Zn = 30/70 atomic ratio and *A* mixed with *H* for Cu/Zn less than 30/70. For Cu/Zn = 0/100 the precursor compound is pure *H*. At higher Cu/Zn ratios *CuHN* is present in the precursor as previously reported by Herman *et al.* (*1*) and Petrini *et al.* (*2*) but *R* is not present in any of the precursors in the whole compositional range. Results and conclusions concerning the precursor identifications are presented in this paper.

EXPERIMENTAL

Sample preparation and analyses. Precursors with atomic ratios of Cu/Zn = 0/100, 10/90, 20/80, and 30/70 were prepared by coprecipitation from copper(II) and zinc(II) nitrate solutions by sodium carbonate addition in a manner described in detail earlier (*1*). In addition, a Cu/Zn = 30/70 precursor was precipitated from a copper(II) and zinc(II) acetate solution by sodium carbonate as follows: 22.60 g of $(CH_3COO)_2Cu \cdot H_2O$ and 56.62 g of $(CH_3COO)_2Zn \cdot 2H_2O$ (both Baker analyzed) were dissolved in 1500 ml distilled water, heated to 85°C, and 1.0 *M* Na_2CO_3 was added dropwise over a 2-hr period, at which time a pH of 7 was reached. After cooling with continuous stirring for 1.5 hr, the precipitate was washed by decantation 3 times, filtered, washed 20 times with 10–20 ml portions of water, and dried in air. Elemental analysis of the Cu/Zn = 30/70 sample yielded 4.43 wt% C, 17.17 wt% Cu, and 41.27 wt% Zn. These weight fractions correspond to the atomic ratios Cu/Zn = 29.98/70.02, close to the theoretical 30/70, and (Cu + Zn)/C = 5.000/2.046, close to the stoichiometric ratio 5/2 for *H* and *A* but different from the stoichiometric ratio 2/1 for *R*.

A sample of the natural mineral *A* was obtained from Wards Natural Science Establishment, and elemental analysis of the sample revealed 4.44 wt% C, 23.94 wt% Cu, and 33.64 wt% Zn. These weight percentages correspond to the atomic ratio (Cu + Zn)/C = 5.000/2.064, close to the stoichiometric ratio 5/2 for *A* and *H*. The elemental analyses reported above were performed by Galbraith Laboratories, Inc., Knoxville, Tennessee.

X-Ray diffraction. The powder diffraction patterns were obtained with a Philips automated X-ray powder diffractometer consisting of an XRG 3100 X-ray generator coupled with an APO 3600 control unit. Scans were taken with a 2θ step size of 0.01° and a counting time of 1.2 sec using CuK_α radiation. Structural data for *H*, *A*, *R*, and *CuHN* were taken from the literature (*3*, *5*, *6*)[1] and are summarized in Table 1.

Electron microscopy. A Philips 400T electron microscope was used for particle imaging, SAD, CBD in the TEM mode, and EDS analyses in the STEM mode. A 120-kV accelerating voltage was used in all analyses. A spot size of 10 nm and counting time of 100 sec were used in the STEM analysis. The Cu/Zn ratios were determined quantitatively from integrated EDS intensities using the thin-film approximately and the value of $k_{Cu/Zn} = 0.956$ as in Ref. (*7*).

RESULTS

Cu/Zn = 30/70 precursor. The X-ray diffraction patterns of the precursors precipitated from the nitrate and acetate solutions were identical, and an example from the nitrate preparation is given in Fig. 1a and Table 2. The XRD pattern matches that of *A* given by Jambor and Pouliot (*3*) but is different from *H* (*3*) or *R* (*5*). For example, the intense lines at 2θ = 34.1°, 41.9°, and 50.1° are characteristic of *A*, and the absence of *R* lines at 14.7° and 17.3° and of *H* lines at

[1] The latter reference in Ref. (*5*) gives crystal structure data for $Cu_2CO_3(OH)_2$ which is isomorphous with $(Cu,Zn)_2CO_3(OH)_2$.

TABLE 1

Literature Data for Cu and Zn Hydroxycarbonate and Nitrate Compounds

	Hydrozincite	Aurichalcite	Rosasite	Copper hydroxide nitrate
Formula	$Zn_5(CO_3)_2(OH)_6$[a]	$(Cu,Zn)_5(CO_3)_2(OH)_6$	$(Cu,Zn)_2CO_3(OH)_2$	$Cu_2(OH)_3NO_3$
Symbol	*H*	*A*	*R*	*CuHN*
Crystal system	Monoclinic	Orthorhombic	Monoclinic	Monoclinic
Space group	$C2/m$	$B22_12$	$P2_1/a$	$P2_1/m$
Unit cell dimensions (nm)				
a_0	1.358	2.72	0.94	0.5605
b_0	0.628	0.641	1.23	0.6087
c_0	0.541	0.529	0.34	0.6929
β	95°35′		≈90°	94°29′
Reference	(*3*)	(*3*)	(*5*)	(*6*)

[a] Substitution of Cu for Zn has been postulated to occur in hydrozincite (*2*, *3*).

47.5° and 51.5°, all of which are intense in their respective compounds, demonstrates that the Cu/Zn = 30/70 precursor is predominantly a single-phase *A*.

XRD data of the Ward mineral *A* are given in Table 2, and all the lines except the weak reflection having d = 1.33 nm match the reported values for *A* (*3*). The additional line corresponds to the *A*{200} reflections. This line could not be accounted for by the *H* structure because it would correspond to the *H*{100} reflections which are forbidden in the $C2/m$ monoclinic space group (*5*). The unit cell volume of the natural mineral *A* was 1.6% smaller than that of *A* in the synthetic sample and 1.9% smaller than the value calculated from the data of Jambor and Pouliot (*3*). The smaller lattice dimensions of the mineral *A* can be accounted for by its higher copper-to-zinc ratio (Cu/Zn = 42/58), as compared to the synthetic sample (Cu/Zn = 30/70) and the literature (Cu/Zn = 29/71 (*3*)).

Further details of the structure and morphology of the Cu/Zn precursors were obtained from transmission electron microscopy including SAD, CBD, and STEM-EDS analyses of single particles. A single phase was observed in the synthetic Cu/Zn = 30/70 sample which had a platelet morphology (Fig. 2a). A similar platelet morphology was found in the natural mineral *A* (Fig. 3a). Platelets in the *A* mineral could be found with lateral dimensions

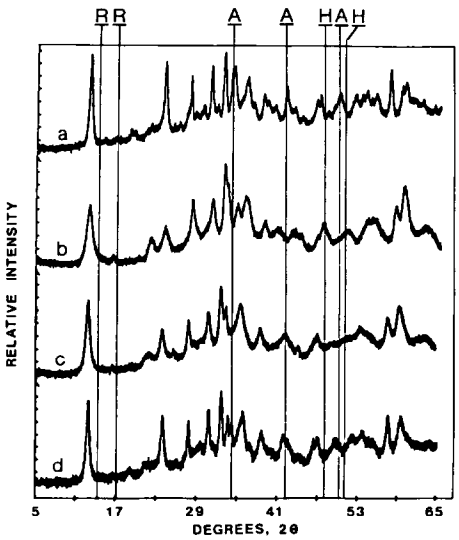

FIG. 1. X-Ray powder diffraction patterns of the catalyst precursors having Cu/Zn atomic ratios of (a) 30/70, (b) 0/100, (c) 10/90, and (d) 20/80. Diffraction lines useful for distinguishing rosasite (*R*), aurichalcite (*A*), and hydrozincite (*H*) are shown as vertical lines marked by the symbols of the respective structures.

TABLE 2

d-Spacings and Intensities from X-Ray Powder Diffraction Patterns of Cu/Zn Catalyst Precursors[a]

Cu/Zn = 30/70		Cu/Zn = 0/100		Cu/Zn = 10/90		Cu/Zn = 20/80		Cu/Zn = 42/58[b]	
d(nm)	$\%I_0$	*d*(nm)	$\%I_0$	*d*(nm)	$\%I_0$	*d*(nm)	$\%I_0$	*d*(nm)	$\%I_0$
0.679	100	0.680	47	0.682	89	0.680	91	1.33	1
0.579	1	0.535	3	0.535	2	0.462	2	0.671	100
0.528	1	0.406	12	0.404	10	0.404	4	0.576	<1
0.467	2	0.370	18	0.371	32	0.370	54	0.505	<1
0.455	2	0.317	46	0.347	9	0.320	48	0.465	1
0.404	4	0.288	44	0.320	42	0.302	6	0.450	3
0.370	76	0.273	100	0.290	50	0.290	69	0.403	<1
0.340	4	0.269	63	0.274	100	0.274	100	0.377	1
0.326	11	0.258	30	0.268	57	0.267	59	0.369	13
0.320	56	0.250	44	0.253	61	0.262	43	0.338	4
0.314	2	0.232	11	0.234	17	0.250	59	0.325	2
0.302	8	0.216	8	0.213	15	0.244	10	0.320	1
0.290	67	0.210	8	0.205	5	0.234	30	0.312	3
0.282	6	0.205	6	0.192	13	0.215	27	0.299	2
0.274	90	0.192	17	0.171	17	0.205	3	0.290	3
0.263	66	0.178	10	0.160	39	0.195	19	0.281	3
0.250	41	0.170	19	0.156	57	0.193	21	0.275	2
0.242	15	0.167	19	0.147	10	0.183	23	0.272	3
0.234	24	0.159	31			0.175	25	0.271	2
0.228	18	0.155	59			0.170	20	0.262	7
0.224	12	0.148	16			0.160	49	0.246	2
0.216	33					0.155	41	0.242	4
0.210	13					0.145	3	0.233	2
0.209	6							0.228	1
0.198	18							0.226	2
0.195	23							0.224	2
0.189	5							0.210	1
0.185	8							0.208	1
0.182	21							0.198	1
0.181	10							0.195	2
0.175	18							0.194	3
0.172	20							0.190	1
0.169	23							0.185	1
0.161	45							0.183	2
								0.176	<1
								0.175	1
								0.171	1
								0.169	7

[a] Intensities were approximated from peak heights.

[b] The aurichalcite mineral sample obtained from Wards Natural Science Establishment.

across the platelet surface up to 0.1 mm, whereas in the synthetic sample the largest platelets observed had dimensions on the order of 1 μm.

SAD patterns from the synthetic and the natural mineral samples, taken with the platelet surface approximately perpendicular to the electron beam, are given in Figs. 2b and 3b, respectively. The patterns are essentially identical which suggests that the two samples have the same structure. The lattice spacings calculated from 15 SAD patterns from the synthetic sample yielded 0.641 ± 0.004 and 0.531 ± 0.004 nm in two

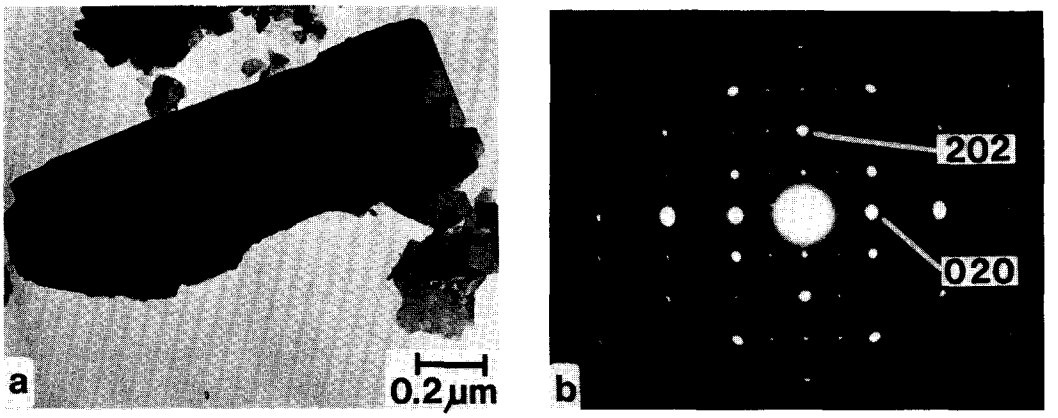

FIG. 2. Electron micrographs of the Cu/Zn = 30/70 catalyst precursor. (a) Bright field image. (b) Selected areas diffraction pattern indexed with respect to the [10$\bar{1}$] zone axis.

orthogonal directions. These values match the b_0 and c_0 unit cell dimensions of *A* (compare with Table 1), and indicate that the observed SAD pattern could be produced from a zone axis near [100]. An accurate determination of the platelet orientation was difficult in the SAD mode because of the close spacings of diffraction spots in the [100] direction. An additional uncertainty arose from diffraction spot broadening in the direction parallel to the electron beam. To resolve the orientation precisely, further diffraction information was obtained with the use of CBD methods (*8, 9*). The natural mineral sample was used rather than the synthetic sample because its thicker platelets enabled the Kikuchi bands and large-radius CBD patterns to be recorded. A CBD pattern from a platelet of mineral *A* is given in Fig. 4a, which was produced by slightly tilting the crystallite to an exact zone axis. This is shown by the symmetric nature of the Kikuchi bands and of the First-Order Laue Zone (FOLZ).

The analysis of the FOLZ ring was carried out with the use of Steed's relation $H = \lambda G^2/2$, where H is the reciprocal lattice layer spacing parallel to the electron beam, λ is the electron beam wavelength, and G is the radius of the FOLZ ring (*9*). The value of H determined from the FOLZ ring in Fig. 4a is 0.725 nm^{-1}, which corresponds to a

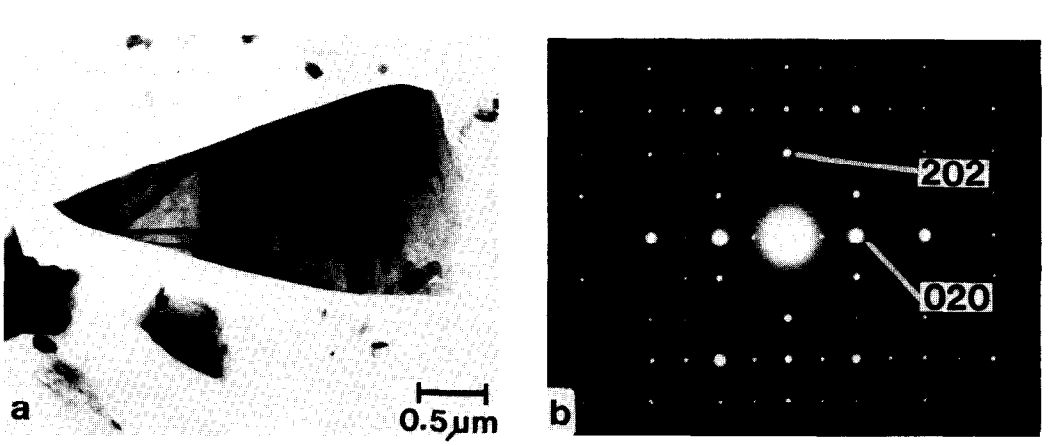

FIG. 3. Electron micrographs of the natural aurichalcite mineral. (a) Bright field image. (b) Selected area diffraction pattern indexed with respect to the [10$\bar{1}$] zone axis.

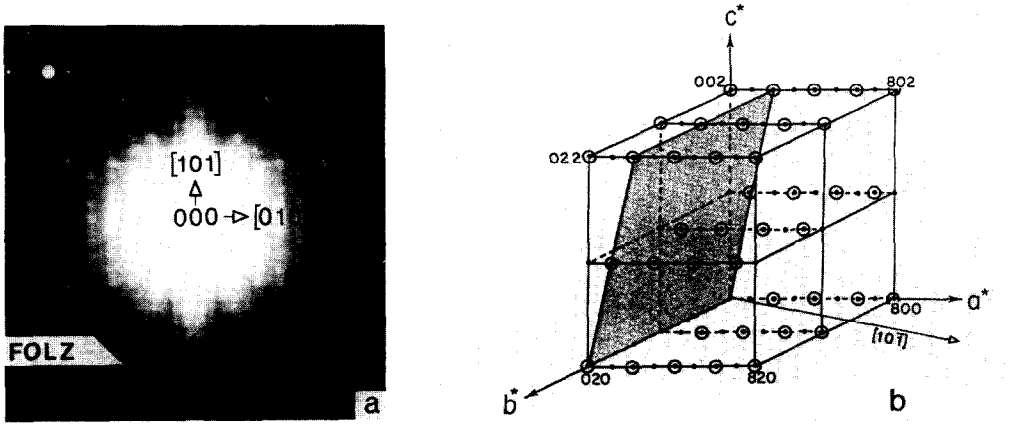

FIG. 4. (a) Convergent beam (20 nm) electron diffraction pattern of a mineral aurichalcite platelet with the [10$\bar{1}$] zone axis showing the FOLZ (First-Order Laue Zone). Inset: the corresponding ZOLZ (Zero-Order Laue Zone) selected area diffraction pattern. (b) Schematic diagram of the reciprocal lattice of aurichalcite where the circled points correspond to the allowed diffraction spots (*3*). The reciprocal lattice plane corresponding to the [10$\bar{1}$] zone axis is shaded.

crystal dimension parallel to the electron beam of H^{-1} = 1.38 nm. This measured value of H^{-1} is close to that calculated for a [10$\bar{1}$] zone axis, 1.36 nm. For the [100] zone axis, however, the calculated H^{-1} spacing would be 2.68 nm and the FOLZ ring would consist of {1*kl*} spots with *l* odd. A FOLZ ring corresponding to the [100] zone axis was not observed, as is evident from Fig. 4a, and therefore the zone axis is [10$\bar{1}$]. The reciprocal lattice of the *A* structure is represented in Fig. 4b with the reciprocal lattice plane perpendicular to the [10$\bar{1}$] zone axis shaded. This figure illustrates that the observed H^{-1} distance of 1.38 nm originates from the alternating allowed and forbidden reciprocal lattice layers perpendicular to the [10$\bar{1}$] axis.

All the diffraction spots in Figs. 2b, 3b, and 4a are consistent with the [10$\bar{1}$] zone axis of *A* as indexed, except for spots of the type (0*k*0) with *k* odd which could be produced by double diffraction. These diffraction patterns cannot be indexed to the monoclinic *H* structure and, therefore, rule out the possibility that *H* was present. For example, to account for the observed diffraction spots with the *H* structure, a zone axis of [$\bar{1}$10] would have to be assumed, but in this case an angle of 87.7° would be present between the [001] and [110] directions and this was not observed.

The elemental composition in the platelets of the Cu/Zn = 30/70 precursor was determined in the STEM-EDS mode, and for 43 measurements the Cu (at.%) = 32.4 ± 3.4 and Zn (at.%) = 67.6 ± 3.4. This result shows that there was a uniform distribution of copper and zinc in the catalyst on a 10-nm scale.

Precursors with Cu/Zn < 30/70. The X-ray diffraction patterns of the precursors with the Cu/Zn = 0/100, 10/90, and 20/80 are presented in Figs. 1b, c, and d, and in Table 2, respectively. The diffraction pattern of the copper-free compound in Fig. 1b and Table 2 is that of *H* with lattice spacings in agreement with those reported by Jambor and Pouliot (*3*) to within 1%. The reflections particularly distinguishing *H* from *A* and *R* are at 2θ = 51.5° and 47.5°. The characteristic lines of *A* at 2θ = 34.1°, 41.9°, and 50.1°, as well as those of *R* at 14.7° and 17.3°, are absent in this composition.

An electron micrograph of the Cu/Zn = 0/100 sample is given in Fig. 5. The particles had a sheet-like morphology and some

FIG. 5. Electron micrograph of the Cu/Zn = 0/100 catalyst precursor.

were oriented to produce a blade-like appearance. A diffuse SAD ring pattern was produced from these areas which had *d*-spacings of 0.323, 0.294, 0.274, 0.255, and 0.160 nm, close to the values for *H*. Not all the *d*-spacings expected for randomly oriented *H* were observed as follows from a comparison with Table 2. This incomplete set of reflections may have resulted from the partial decomposition of the particles under the electron beam. The particles appeared to have a mottled surface, a feature characteristic of decomposition (*10*).

The compositions that are intermediate between pure *H* (Cu/Zn = 0/100) and *A* (Cu/Zn = 30/70) have XRD patterns with lines near both *H* and *A* (see Table 2 and Fig. 1). Compositions such as Cu/Zn = 10/90 and 20/80 gave patterns that are superpositions of the diffraction patterns of *H* and *A* in the proportion dictated by the elemental composition. An example is given in Fig. 6 in which the diffraction pattern of the Cu/Zn = 10/90 precursor is compared with that of the mechanical mixture of 33% of the Cu/Zn = 30/70 precursor *A* and 67% of the Cu/Zn = 0/100 precursor *H*. The two diffraction patterns compared favorably except for small shifts of the Bragg angles and small differences in intensities. The above analyses show that *H* increases as the Cu concentration decreases below 30 at.%.

The TEM images of the Cu/Zn = 10/90 sample showed that platelets were present which appeared similar to those found in the Cu/Zn = 30/70 precursor (see Fig. 2a). SAD patterns from these platelets could not be distinguished from the patterns obtained in the Cu/Zn = 30/70 precursor (see Fig. 2b). The platelets having an *A* structure are therefore present in the Cu/Zn = 10/90 sample. Elemental analysis of the *A* platelets in the Cu/Zn = 10/90 sample gave Cu (at.%) = 11.9 ± 1.0 and Zn (at.%) = 88.1 ± 1.0 from 10 measurements. In addition to the platelets, the Cu/Zn = 10/90 sample contained the sheet-like morphology *H* observed in the Cu/Zn = 0/100 sample.

DISCUSSION

The XRD, SAD, CBD, and STEM-EDS analyses show that the Cu/Zn = 30/70 precursor is a single-phase *A* with a uniform distribution of the two metallic elements. *A* can be distinguished from *H* as was demonstrated by the comparison of the XRD patterns of these two compounds in Figs. 1a and b, respectively. The XRD reflections particularly useful for distinguishing *H* and *A* structures are: for *A*, $2\theta = 34.1°$ (d = 0.263 nm), 41.9° (d = 0.216 nm), and 50.1° (d = 0.182 nm); and for *H*, $2\theta = 47.5°$ (d =

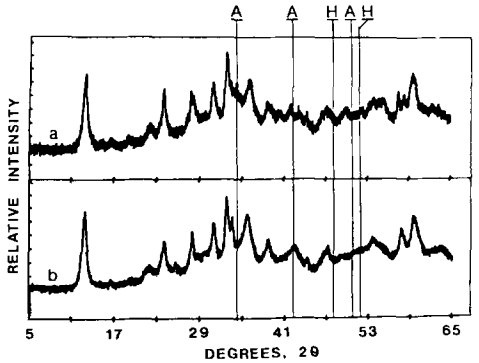

FIG. 6. Comparison of the X-ray powder diffraction pattern obtained (a) from a mechanical mixture of 33% of the Cu/Zn = 30/70 precursor *A* and 67% of the Cu/Zn = 0/100 precursor *H* with that (b) from the Cu/Zn = 10/90 precursor. Diffraction lines useful for distinguishing aurichalcite (*A*) and hydrozincite (*H*) are shown.

0.192 nm) and 51.5° (d = 0.177 nm). The previous assignment of the 30/70 precursor to be a mixture of H and R (*1*) is thereby found to be in error. The identification of the Cu/Zn = 31/69 precursor as a single-phase H (2), however, also is not correct, although H and A are closely related (*11, 12*). A close inspection of the XRD pattern in Ref. (*2*) reveals lines typical of A (sample C31). It is therefore very likely that the Cu/Zn = 30/70 precursor was A in all of the previously reported preparations (*1, 2*) as well as in the present work.

In the range of the Cu/Zn ratios less than 30/70 the precursor is a mixture of A and H but there is some compositional variation within both these structures. The present study showed that the Cu/Zn atomic ratio can vary from 11/89 in the Cu/Zn = 10/90 precipitated precursor to 42/58 in the natural A mineral. This indicates that A forms a continuous solid solution series in this range, in accord with Jambor *et al.* (*3*) that the Cu substitution for Zn in A occurs in a wide compositional range. The proposed complex sheet structure of A (*11, 12*) contains 60% octahedral and 40% tetrahedral sites for the divalent cation. It is well known that zinc ions prefer the tetrahedral coordination and the blue color of the A specimens indicates that the cupric ions occupy preferentially the octahedral holes. Apparently the substitution of Cu for Zn in the octahedral holes can occur over a large range, as observed, while the tetrahedral holes remain occupied by zinc only. In the calcination stage of the catalyst preparation, the precursor A is decomposed to form cupric oxide and zinc oxide. During the thermal decomposition the zinc oxide may be envisaged to nucleate from the arrays of tetrahedral coordination units, while the cupric oxide with local square planar environment will nucleate from the octahedral layers. The tetrahedral and octahedral layers alternate in the [100] direction, and this intimate mixing of the copper and zinc oxide precursor sites results in the fine interdispersion of CuO and ZnO in the calcined catalyst. The decomposition has indeed been shown to proceed along defined crystallographic directions in A and to produce a high dispersion of the oxides (*13*). It is noted that the Cu/ZnO = 30/70 is the most active catalyst for the low-temperature–low-pressure methanol synthesis in the binary copper–zinc oxide series (*1*) and that the Cu/Zn = 30/70 single-phase A precursor gives rise to this high activity.

Interestingly, both aurichalcite and rosasite are formed with nearly the same standard free energy per metal cation (*14*)[2] and the two compounds appear as minerals in the same natural locations. It is quite possible, therefore, that the laboratory preparations can be steered to aurichalcite or to rosasite by a change in preparation conditions. Because the copper and zinc ions are finely interdispersed in both aurichalcite and rosasite, both of these compounds may be viable precursors of active methanol synthesis catalysts.

ACKNOWLEDGMENTS

This research was supported by the U.S. Department of Energy Grant DE-FG22-83PC0786 and by NSF Grant INT-8212842.

REFERENCES

1. Herman, R. G., Klier, K., Simmons, G. W., Finn, B. P., Bulko, J. B., and Kobylinski, T. P., *J. Catal.* **56,** 407 (1979).
2. Petrini, G., Montino, F., Bossi, A., and Garbassi, G., *in* "Studies in Surface Science and Catalysis. Preparation of Catalysis III" (G. Poncelet, P. Grange, and P. A. Jacobs, Eds.), Vol. 16, p. 735. Elsevier, The Netherlands, 1983.
3. Jambor, J. L., and Pouliot, G., *Can. Mineral.* **8,** 385 (1965); X-Ray Powder Data File, ASTM 19-1458 (for hydrozincite) and ASTM 17-743 (for aurichalcite). Jambor, J. L., and MacGregor, I. D., *Geol. Surv. Can.* **B74** (2), 172 (1974).

[2] This reference gives −1100 kcal/mol of rosasite $Cu_{1.16}Zn_{0.84}CO_3(OH)_2$ and −2766 kcal/mol of aurichalcite $Cu_{2.27}Zn_{2.73}(CO_3)_2(OH)_6$, which yields −550 and −553 kcal/g atom of metal, respectively. The free energies of formation depend somewhat on the Cu/Zn ratio, but both R and A are increasingly stable with the increasing content of zinc, as indicated by an extrapolation of the free energies of formation for zinc-free malachite and rosasite and for pure hydozincite and aurichalcite, as given in this reference.

4. Busetto, C., Del Piero, G., Manara, G., Trifiro, F., and Vacari, A., *J. Catal.* **85,** 260 (1984).
5. X-Ray Powder Data File, ASTM 18-1095; A. F. Wells, *Acta Crystallogr.* **4,** 200 (1951).
6. X-Ray Powder Data File, ASTM 15-14.
7. Cliff, G., and Lorimer, G. W., "Proceedings, 5th European Congress EM," pp. 140–141. Institute of Physics, London, 1972.
8. Williams, D. B., *Norelco Rep.* **30**(2), 24 (1983).
9. Steeds, J. W., *in* "Introduction to Analytical Electron Microscopy" (J. J. Hren, J. I. Goldstein, and D. C. Joy, Eds.), p. 387. Plenum, New York, 1979.
10. Herman, R. G., and Domínguez, J. M., *Mater. Res. Bull.* **19,** 905 (1984).
11. Ghose, S., *Acta Crystallogr.* **17,** 1051 (1964).
12. Povarennykh, A. S., "Crystal Chemical Classification of Minerals," Vol. 2, pp. 616–617. Plenum, New York, 1972.
13. Himelfarb, P. B., Simmons, G. W., Klier, K., and Yacamán, M. J., *in* "New Surface Science in Catalysis," Symposium of the 188th National ACS Meeting, Philadelphia, Pa., in press.
14. Alwan, K. A., Thomas, J. H., and Williams, P. A., *Transition Met. Chem. (N.Y.)* **5,** 3 (1980).